Electric Vehicle HV-DC EMC Filter Loss due to Variations in AC-Load Configuration

Lennart P. P. B. Bohl[#1], Guido A. Rasek[*], Mohamed Abdallah[$], Cheng Yang[#], Christian Schuster[#]

[#]Institut für Theoretische Elektrotechnik, Hamburg University of Technology (TUHH), Hamburg, Germany

[*]EMC Architecture Valeo Power Division, Valeo eAutomotive Germany GmbH, Erlangen, Germany

[$]Department of Electronics, Information and Bioengineering, Politecnico di Milano, Milan, Italy

[1]lennart.bohl@tuhh.de

***Abstract* — The motor of an electric vehicle is connected to the inverter either by cables or busbars if the inverter and motor are integrated in the same housing. Instead of a motor, an equivalent lumped load may be used during EMC pre-compliance testing. Utilizing a SPICE-based simulation model, the conducted emissions of an electric vehicle powertrain are investigated with different AC-load configurations. Shielded AC-cables lead to increased parasitic inductance and capacitance on the AC side of the powertrain. On the HV-DC side of the inverter, EMC filters are required to comply with conducted emissions limits. The filter components, especially those filtering the common mode, are exposed to power loss due to the noise currents on the powertrain. Simulation results for AC-cable lengths 0-3 m show that the power loss in the EMC filter components shows a strong dependency on cable length.**

***Keywords* — conducted emissions, electric motors, electric vehicles, electromagnetic compatibility, passive filters, shielded cables**

I. Introduction

Fast switching, high currents as well as weight and space requirements in modern electric vehicles (EVs) are challenging for electromagnetic compatibility (EMC) compliant design. The inherent high-frequency harmonics, excited due to the switching of the inverter, lead to noise currents on the high-voltage (HV) powertrain. To stay below standardized or system required limits, EMC filters have to be used. Otherwise, on the DC side of the inverter, the emissions may interfere with other electronic systems like the battery management system or radiate off the cables. Regarding the emissions, especially the common mode (CM) emissions, the AC-load plays a crucial role [1]. Any capacitance from the three-phase system to the chassis will lead to CM currents. In an EV the AC-load is the e-motor. During development, motor equivalents, built up from a minimal set of lumped parts may be used instead of a motor for pre-compliance measurements [2], [3], e.g. if the motor is not available. Such an equivalent load may be made up from off-the-shelf components and aims to represent the low frequency behavior of the e-motor.

The second component on the AC domain of the powertrain are AC-cables. Cables in the EV powertrain may be shielded or unshielded. To conform with radiated emissions requirements as well as to limit human exposure to non-ionizing radiation, often shielded cables are used. Depending on the specific vehicle, the length of the AC-cables may vary significantly.

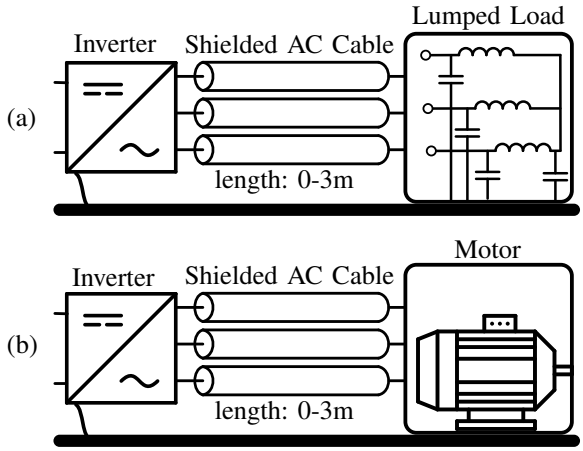

Fig. 1. AC-load configurations of an electric vehicle with shielded AC-cables above a reference ground plane. a) configuration with a lumped capacitive and inductive equivalent load for pre-compliance testing. b) configuration with an e-motor.

AC-cables may be completely omitted by using an electric axle, where motor and inverter are integrated in the same housing. In EVs where inverter and motor have to be spaced far apart, long AC-cables have to be used. Examples are industrial vehicles or buses, where the inverter may be placed on the roof. Furthermore, during testing of prototypes or early samples in development, cables may be used for individual testing of an inverter or e-motor before the final integration, e.g., to test a next generation motor with a previous generation inverter. AC-cables that are longer than intended in the final system may also be used for convenience of placement of components on the test bench or limited availability of shorter cables.

The HV-DC EMC filter is located within the inverter housing on the DC-side. The filter components are exposed to stress due to power loss and subsequent self-heating [4], [5]. The AC-load plays an important role regarding the conducted emissions [6] and therefore the loss in the EMC filter components. To study this effect in the context of an EV powertrain, variations of the AC-powertrain are investigated herein. The variations are indicated in Fig. 1. Figure 2 shows the influence of two different AC-load configurations on the conducted emissions in measurements.

The remainder of this paper is organized as follows: Section II introduces the EV powertrain components with a

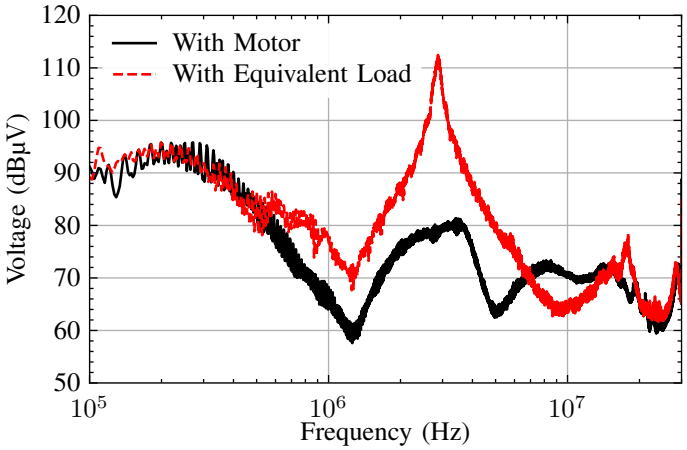

Fig. 2. Measured conducted emissions of an EV powertrain at the HV-DC LISN. The configuration with the motor is in an electric-axle configuration, where the inverter and motor are integrated in the same housing and no AC-cable is used. AC-cable length for the measurements with equivalent load $\approx 0.75\,\mathrm{m}$.

focus on the AC components. Section III describes the HV-DC EMC filter. Section IV shows the results of a parametric study of the AC-cable length with two different AC-loads. The effects are evaluated in terms of power loss in the EMC filter components and conducted emissions. Section V provides conclusions regarding the investigated configurations.

II. Electric Vehicle Powertrain

The EV powertrain under investigation has a nominal DC-Voltage of 350 V and a 10 kHz pulse width modulation (PWM) switching frequency of the inverter. All three half-bridges are switched at the same time and to the same voltage, which superimposes the CM noise currents. This operation mode corresponds to the maximum EMC filter CM power loss [5].

A. Simulation Model

A SPICE-based circuit simulation is utilized to acquire the time domain conducted emissions voltages at the line impedance stabilization network (LISN). The model has been verified and shown good agreement with measurements [7]. The model includes all relevant components of an EV powertrain in an EMC test setup. Those are: the LISN, shielded DC-cables, inverter, shielded AC-cables, and three-phase load.

B. Shielded AC-Cables

As indicated in Fig. 1 three individually shielded cables are investigated. Individually shielded cables are common in EVs because of advantages in mechanical integration and handling. The shielded cable parameters and geometry are taken from [8]. The cable model is based on [9] which has been implemented in a powertrain simulation in [10]. The circuit model for a Δx-long section of a single-phase shielded AC-cable is shown in Fig. 3. Each AC-cable is modeled as a three conductor system consisting of the inner conductor, the shield, and the reference ground, which is the conductive ground table. Path resistances are induced for

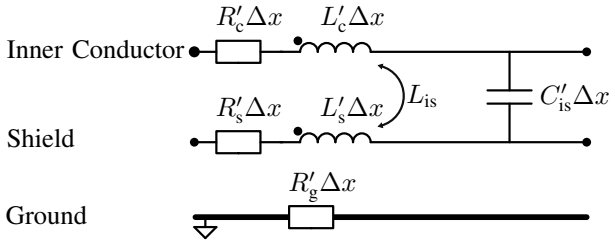

Fig. 3. Equivalent circuit for a Δx-long section of a single shielded AC cable. For the three-phase circuit mutual inductance between all shields and conductors are considered.

each conductor. The inner conductor and shield inductance are calculated in reference to the ground table. The component values are calculated by multiplication of the per-unit-length (p.u.l.) values and the Δx segment length. To ensure electrical short behavior at the maximum frequency of investigation, Δx is set to be a maximum of 0.75 m. Multiple sections are cascaded to model longer cable lengths. The p.u.l. inductance of the cable L'_c is given by [11]

$$L'_c = \frac{\mu_0}{2\pi} \ln\left(\frac{2h_R}{r_\mathrm{c}}\right) \tag{1}$$

and shield L'_s

$$L'_s = \frac{\mu_0}{2\pi} \ln\left(\frac{2h_R}{r_\mathrm{s}}\right), \tag{2}$$

where μ_0 denotes the free space permeability, h_R the height of the cable over the ground plate. r_c and r_s denote the radius of the center conductor and outside of the shield, respectively. The p.u.l. mutual inductance L'_{is} of shield and cable is equal to the shield inductance $L'_{cs} = L'_s$. The p.u.l. mutual inductance L'_m between each conductor or shield u to any other conductor or shield v is calculated from the assumption of two wires above ground by [11]

$$L'_{m,uv} = \frac{\mu_0}{2\pi} \ln\left(1 + \frac{4h_R^2}{s^2}\right), \tag{3}$$

where s denotes the distance between the center point of the conductors. In the three-phase system, coupling between all conductors and shields is considered.

The p.u.l. capacitance C_is between the inner conductor and shield can be calculated [11] or taken from the data sheet [8]. Capacitances between the shield and ground as well as shield-shield are not included. All shields are shorted at their ends towards ground. This significantly diminishes the effect of the shield-shield and shield-ground capacitance. Simulation runs including the full capacitance matrix show no notable change regarding filter loss or conducted emissions in the frequency range of interest (<30 MHz). In order to keep model complexity low, they are omitted. The p.u.l. resistances $R'_\mathrm{c}, R'_\mathrm{s}, R'_\mathrm{g}$ can be estimated analytically [11] or extracted from measurements [9].

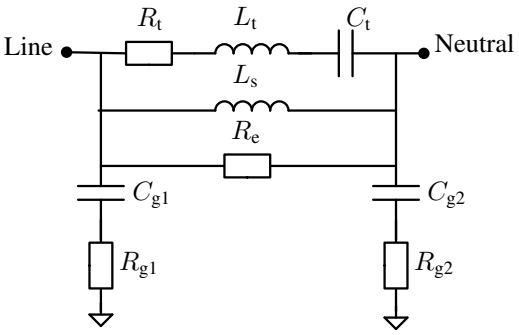

Fig. 4. Equivalent circuit for a single phase of the motor proposed in [12]. For the three-phase circuit, the mutual inductance between the windings L_s of all phases are considered.

C. Electric Motor

In literature, multiple equivalent circuits are proposed to model the electrical behavior of an electric motor [12], [13], [14]. Therein, extraction procedures are discussed to acquire the values of equivalent circuit components. Following the proposed model and parameter extraction procedure in [12], the model in Fig. 4 is used to acquire the simulation model from a measured permanent-magnet synchronous motor (PMSM).

The parameters used in the model possess a physical meaning. As argued in [12], L_s represents the stator winding inductance. R_e expresses the high-frequency eddy current losses inside the magnetic core and frame. C_{g1} represents the parasitic capacitance between the phase winding and the stator frame. C_{g2} represents the parasitic capacitance between the neutral and the stator frame. R_{g1} and R_{g2} are the equivalent resistances for the copper skin effect. The parallel $R_t L_t C_t$ branch accounts for stator winding inter-turn effects.

The resulting fit of measurement and simulation regarding the CM and differential mode (DM) impedance is shown in Fig. 5. Measurement and simulation show good agreement regarding the CM impedance up to 30 MHz. The DM shows minor deviations. As the filter components under investigation are predominantly exposed to CM noise, the model to measurement correlation is deemed sufficient. Fig. 5 shows the impedance of the equivalent load for the three-phase CM and phase-to-phase DM. The low-frequency inductive and capacitive behavior are comparable between motor and equivalent load. The first anti-resonance of the CM impedance is at a higher frequency in the equivalent load. All resonances of the equivalent load are of high quality factor, as the equivalent load lumped components have very little damping.

III. HV-DC EMC Filter

The HV-DC EMC filter is made up of a single stage of C_y and C_x capacitors as well as a choke. The filter is positioned in the DC domain of the powertrain. It is integrated into the inverter-housing and aims to minimize noise on the DC-cables. A circuit diagram of the EMC filter is shown in Fig. 6. The electrical behavior of the filter components as well as the loss calculation procedure for the filter components is presented.

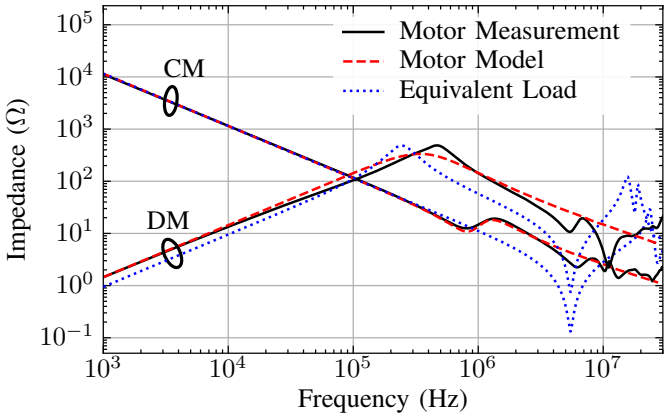

Fig. 5. CM impedance (three-phase) and DM impedance (phase-to-phase) of the measured PMSM motor, the motor model and the equivalent load.

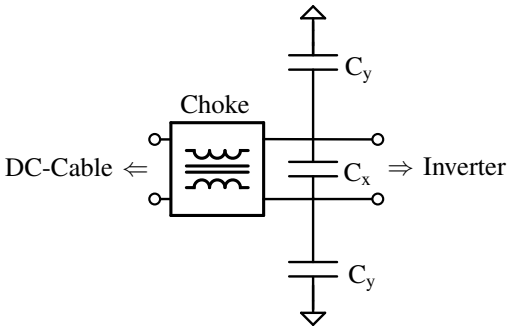

Fig. 6. Single stage HV-DC EMC filter.

A. Capacitors

In the EMC filter, a single stage of C_y and C_x capacitors is used. The capacitors are film capacitors. An emphasis is set on the C_y capacitors in this section as they filter the CM which is the dominant part of the emissions in the herein investigated frequency range and the C_y capacitors have higher power loss than the C_x capacitors [5]. The C_y capacitance is 220 nF. The capacitors are modeled as a series connection of an ideal capacitance, an equivalent series resistance (ESR) and an equivalent series inductance (ESL) [15]. The measured frequency-dependent impedance and ESR are shown in Fig. 7.

To accurately calculate the loss in the C_y capacitors, the frequency-dependent ESR has to be considered [4], [5]. Therefore, time-dependent current through the capacitor is transformed to the frequency domain and multiplied by the frequency-dependent ESR. The power is calculated from the frequency domain integral over the current through the capacitor squared and scaled with the ESR [5].

B. Choke

The choke is made from a nano-crystalline material. The busbar runs through two slots in the choke which leads to a CM inductance. Figure 8 shows the measured impedance of the choke over frequency. Additionally, the real part of the impedance, which corresponds to the frequency-dependent resistance and therefore the loss-behavior is shown.

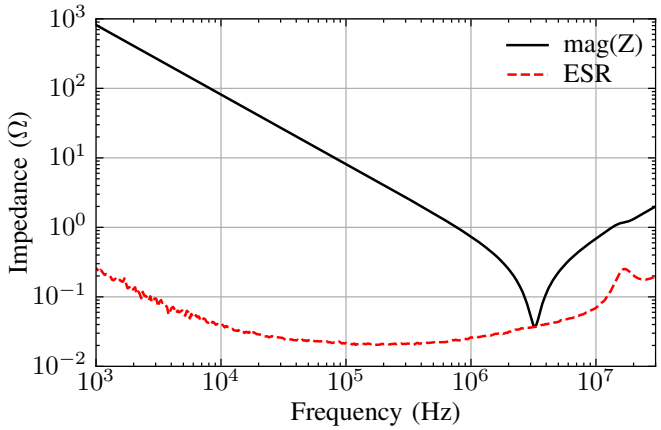

Fig. 7. Measured impedance and ESR of a 220 nF C_y capacitor.

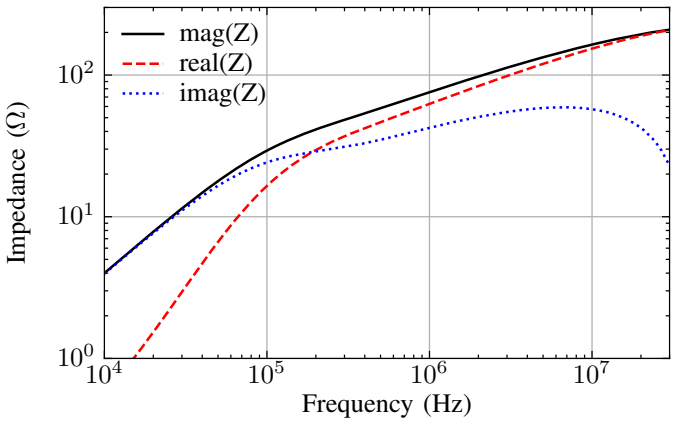

Fig. 8. Measured CM impedance of the choke and its real and imaginary components. The frequency-dependent real part of the impedance is related to the loss in the choke.

The simulation model of the choke consists of cascaded sets of parallel inductance and resistance elements. Their values are fitted to the measurement data [16]. Thereby, the frequency-dependent inductance and resistance of the choke are represented in the time domain simulation. Saturation effects are not represented. The loss in the choke is calculated in the time domain [5].

IV. Parametric Study of the AC-Cable Length

The configurations shown in Fig. 1 are simulated and the results are evaluated regarding the power loss in the EMC filter components as well as the conducted emissions at the HV-DC LISN.

A. Power Loss in the HV-DC Filter

The EMC filter stress is investigated by the power loss in the filter components. The loss in the choke and a C_y capacitor is shown in Fig. 9 for different AC-cable lengths. For both filter components, the loss increases when increasing the AC-cable length. An increase from 32 mW to 135 mW in terms of power loss in the C_y can be observed in the configuration with a motor, when increasing the length from 0 m to 3 m. With an equivalent load, the increase is from 0.646 W to 1.5 W.

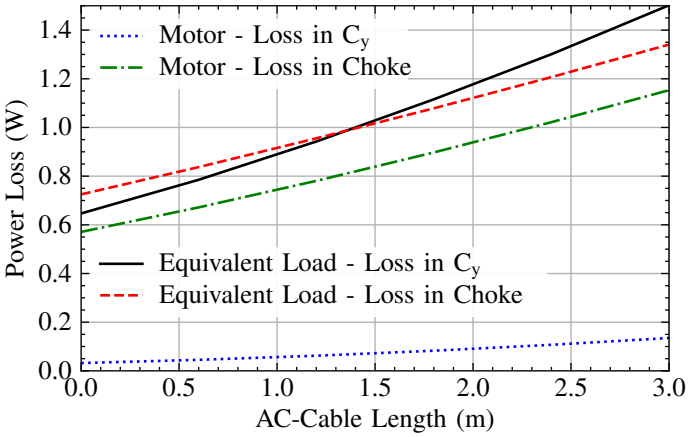

Fig. 9. Losses in filter components with equivalent load and motor over AC-cable length.

The loss in the choke increases by 0.58 W in case of a motor and by 0.62 W in case of an equivalent load when the cable length is increased from 0 to 3 m. The loss in the choke diverges less than the loss in C_y when exchanging the equivalent load for a motor.

1) Frequency-dependent Loss of the C_y Capacitor

To further analyze the effect of the AC-cable on the loss in the C_y capacitors, Fig. 10a and Fig. 10b depict the frequency-domain cumulative loss (which is the cumulative integration of the frequency dependent loss) in the C_y capacitor. The cumulative loss shows the effect of the frequency-dependence of the current through the capacitor and the frequency-dependence of the ESR. For all configurations, no increase in loss above 6 MHz is observed. The resonance around 3 MHz leads to the majority of loss. For longer AC-cables the loss increases while the resonance frequency decreases. The ESR shown in Fig. 7 shows a reduction of ESR for a reduction in frequency within the frequency range of interest. This implies a reduction of loss in the C_y. The additional capacitance to ground introduced by the AC-cable leads to an increase in loss. This effect is dominant over the change in resonance frequency and ESR.

2) Frequency-dependent Loss of the Choke

In contrast to the loss in the C_y capacitor, the choke has only 20% less loss when comparing the motor to the equivalent load. Figure 11 shows the cumulative loss in the choke for the configuration with equivalent load and motor. The cumulative loss is equal for both configurations up to 2 MHz. With the equivalent load, 0.28 W of loss can be attributed to the resonance around 3 MHz. In the case with a motor this is 0.02 W. The majority of loss in the choke is due to loss in the frequency range 10 kHz to 200 kHz. The discrete steps in the power loss stem from the fundamental switching frequency of the inverter, which is 10 kHz. The superposition of the switching waveforms on the three-phase system leads to only odd multiples of the switching frequency being excited.

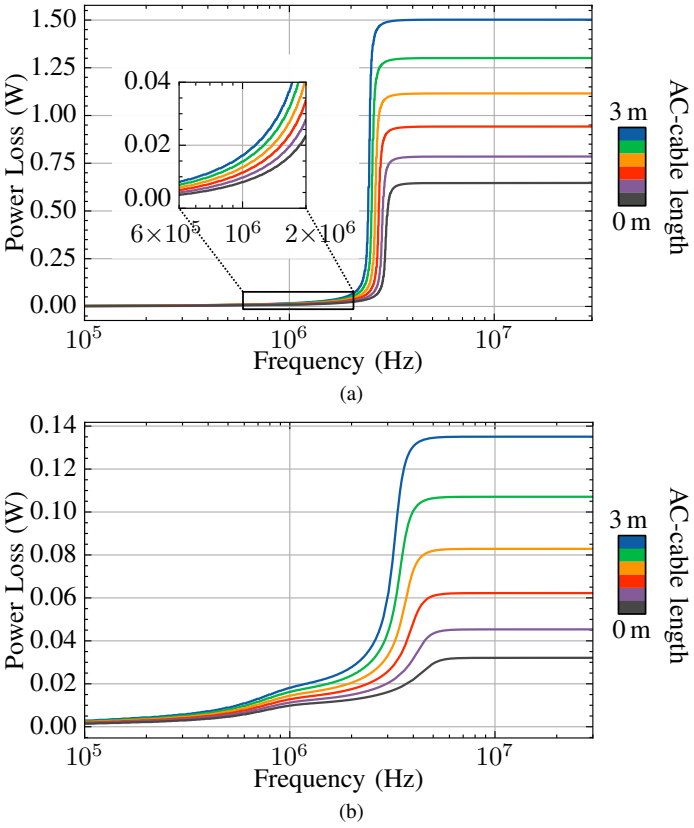

Fig. 10. Cumulative loss over frequency in C_y for different AC-cable lengths (0-3 m). a) with an equivalent load. b) with a motor.

The real impedance of the choke in Fig. 8 indicates that a higher frequency of the noise currents (up to 8 MHz) relates to higher loss. But for the calculation of the loss with broadband signals, the frequency-dependence of the noise currents has to be considered. The CM currents though the choke decay for higher frequencies. Therefore, the loss is dominated by low-frequency currents.

B. *Conducted Emissions*

The conducted emissions at the LISN are calculated from the time domain with a software-based EMI receiver (SEMI) [17]. The SEMI receiver applies the frequency-dependent bandwidths and signal post-processing according to regulations [18].

Fig. 12 depicts the conducted emissions at the LISN with the equivalent load and with a motor. The AC-cable length is 0.6 m for both configurations. While the behavior below 1 MHz is similar, the resonance at 2.8 MHz, which has a high quality factor with the equivalent load, is spread out and damped when a motor is used. Furthermore, it is shifted to higher frequencies with a peak at 4 MHz. This follows the effects seen in measurements of a similar powertrain as shown in Fig. 2.

The effect of different AC-cable lengths is shown in Fig. 13a for the equivalent load and in Fig. 13b for the motor configuration. In the frequency range below 1 MHz an increase of up to 3 dB can be observed between 0 m and 3 m. This is similar for both load configurations. With the

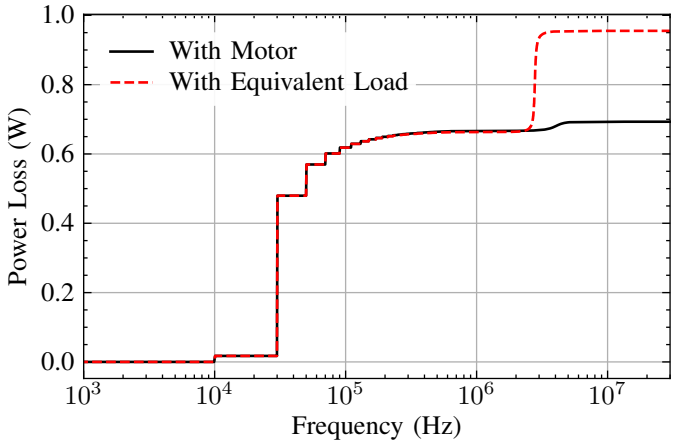

Fig. 11. Cumulative loss in the choke over frequency for a motor and an equivalent load as an AC-load. The AC-cable length is 0.6 m in both cases.

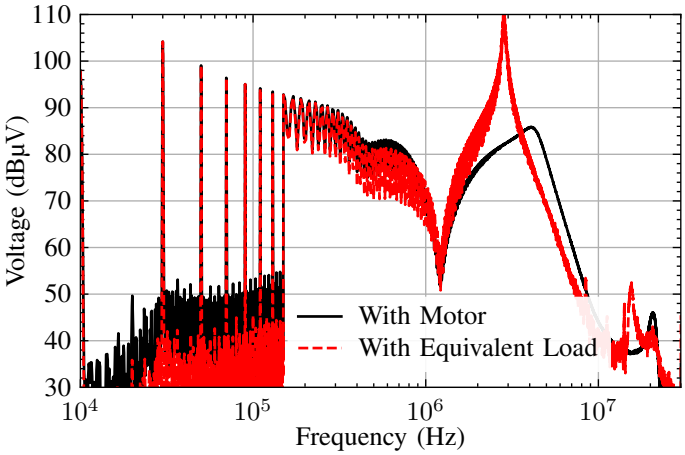

Fig. 12. SEMI receiver and peak algorithm conducted emissions at the LISN with motor and equivalent load. AC-cable length set to 0.6 m in both cases.

equivalent load, a shift in resonance frequency from 4 MHz to 2.3 MHz can be observed, while the resonance peak amplitude increases by 5 dB. The shift in resonance can be explained by the additionally introduced CM inductance and capacitance of the cable, which both reduce the resonance frequency of this resonance. The increase in amplitude is due to the additional capacitance to ground introduced by the AC-cable. With the motor as the load, shown in Fig. 13b, a similar shift in resonance frequency is observed. The amplitude changes up to 14 dB over the lengths of cable investigated.

V. Conclusion

A validated numerical simulation model is utilized to investigate different AC-load configurations for an electric vehicle powertrain. The EMC filter component power loss and conducted emissions are investigated and analyzed. The effects of a lumped equivalent load used in pre-compliance tests are compared to a motor. With knowledge of the influence of the equivalent load, an equivalent load can be used in pre-compliance testing and quantification of emissions below 2 MHz. An equivalent load that better represents the motor

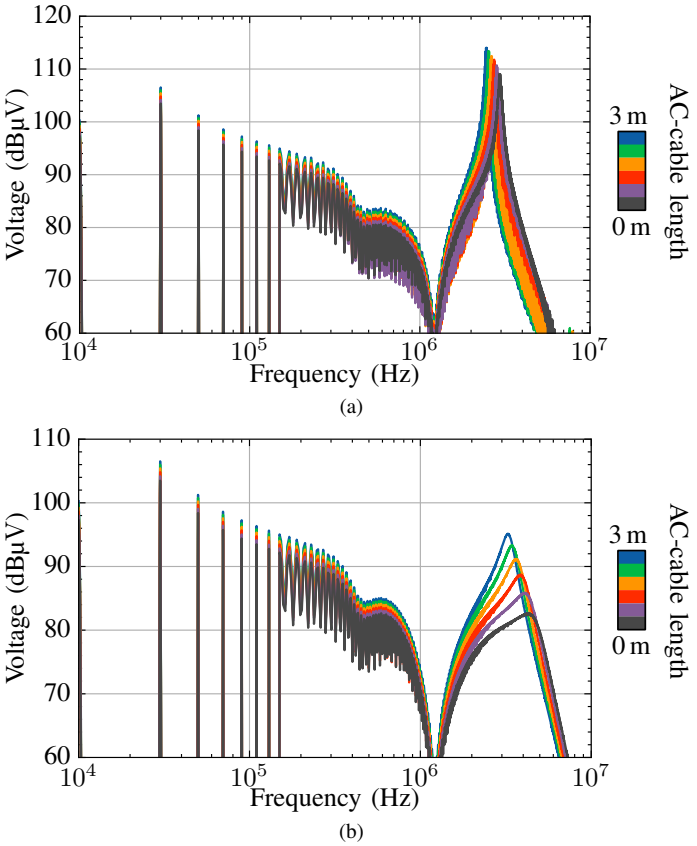

Fig. 13. SEMI receiver and peak algorithm conducted emissions at the LISN as the load for different AC-cable length (0-3 m). a) with an equivalent load. b) with a motor.

model should be used if representative conducted emissions measurements for higher frequencies are required.

Regarding the loss in the EMC filter components due to variation of the load, the following can be concluded: The C_y capacitor loss is strongly influenced by how much resonances in frequency ranges close to the capacitor self resonance are damped. The loss in the choke on the other hand is dominated by the fundamentals of the PWM switching signals. Loss management techniques can take this into account.

Variation of the AC-cable length has a strong impact on the loss in the filter components. This should be kept in mind when designing the filter. Additionally, in component testing AC-cables should be kept to a minimum. When, e.g. for convenience a long cable is chosen for motor or subcomponent testing, overheating and destruction of the filter may occur.

While the variation of the AC-cable length has a similar trend on the conducted emissions for both loads investigated, the strength of the impact differs. A deeper investigation of the relation of load and cable, especially regarding the capacitance to ground, should be performed in future work in order to quantify in what configurations the AC-cable length is a relevant design variable regarding EMC.

References

[1] A. Kempski, R. Smolenski, and R. Strzelecki, "Common mode current paths and their modeling in PWM inverter-fed drives," in *33rd Annual IEEE Power Electronics Specialists Conference*, Cairns, QLD, Australia: IEEE, Jun. 27, 2002. DOI: 10.1109/psec.2002.1022396.

[2] Z. Liu, O. Mohammed, and S. Liu, "Equivalent hardware representation of PM synchronous motors from the physics-based phase variable model obtained through FE computation," *IEEE Transactions on Magnetics*, vol. 45, no. 3, pp. 1450–1453, Mar. 2009, ISSN: 0018-9464. DOI: 10.1109/tmag.2009.2012670.

[3] S. Jeschke et al., "EMI measurement on electric vehicle drive inverters using a passive motor impedance network," in *Asia-Pacific International Symposium on Electromagnetic Compatibility (APEMC)*, Shenzhen, China: IEEE, May 2016. DOI: 10.1109/apemc.2016.7523037.

[4] M. Tranchero, P. Santero, G. Von Pfingsten, and M. Nuotio, "Thermal simulation and optimization of a common-mode filter for a SiC inverter," in *International Symposium on Electromagnetic Compatibility - EMC Europe*, Krakow, Poland, Sep. 2023. DOI: 10.1109/EMCEurope57790.2023.10274169.

[5] L. P. P. B. Bohl, G. A. Rasek, T. Stöhr, C. Yang, and C. Schuster, "Calculation and distribution of losses in EMC filters in the high-voltage power train for an electric vehicle," in *International Symposium on Electromagnetic Compatibility – EMC Europe*, Brugge, Belgium: IEEE, Sep. 2024. DOI: 10.1109/emceurope59828.2024.10722334.

[6] P. Hillenbrand, S. Tenbohlen, C. Keller, and K. Spanos, "Understanding conducted emissions from an automotive inverter using a common-mode model," in *International Symposium on Electromagnetic Compatibility*, IEEE, Aug. 2015, pp. 685–690. DOI: 10.1109/isemc.2015.7256246.

[7] T. Stöhr, G. A. Rasek, and N. S. Murthy, "Agreement quantification of a numerical EMC computer model and test infrastructure for the HV power train emissions for an electric vehicle," in *International Symposium on Electromagnetic Compatibility - EMC Europe*, Krakow, Poland, Sep. 2023. DOI: 10.1109/emceurope57790.2023.10274221.

[8] Coroplast Fritz Müller GmbH & Co. KG, *Technische information coroplast part no.: 9-2611 / 50 mm^2, Klebebänder, Kabel, Leitungssatzsystem*, version A9, 2012.

[9] A. Beltramelli, F. Grassi, G. Spadacini, and S. A. Pignari, "Modeling conducted noise propagation along high-voltage DC power buses for electric vehicle applications," in *International Conference on Connected Vehicles and Expo (ICCVE)*, Vienna, Austria: IEEE, Nov. 2014, pp. 56–61. DOI: 10.1109/iccve.2014.7297611.

[10] K. Wang, H. Lu, C. Chen, and Y. Xiong, "Modeling of system-level conducted EMI of the high-voltage electric drive system in electric vehicles," *IEEE Transactions on Electromagnetic Compatibility*, vol. 64, no. 3, pp. 741–749, Jun. 2022. DOI: 10.1109/temc.2022.3147521.

[11] C. R. Paul, *Introduction to Electromagnetic Compatibility*. Hoboken, New Jersey, USA: Wiley, Sep. 2005.

[12] M. S. Toulabi, L. Wang, L. Bieber, S. Filizadeh, and J. Jatskevich, "A universal high-frequency induction machine model and characterization method for arbitrary stator winding connections," *IEEE Transactions on Energy Conversion*, vol. 34, no. 3, pp. 1164–1177, Jan. 2019. DOI: 10.1109/tec.2019.2891349.

[13] M. Schinkel, S. Weber, S. Guttowski, W. John, and H. Reichl, "Efficient HF modeling and model parameterization of induction machines for time and frequency domain simulations," in *Twenty-First Annual IEEE Applied Power Electronics Conference and Exposition (APEC)*, Dallas, TX, USA: IEEE, Apr. 2006. DOI: 10.1109/apec.2006.1620689.

[14] O. Mohammed, S. Ganu, N. Abed, S. Liu, and Z. Liu, "High frequency PM synchronous motor model determined by FE analysis," *IEEE Transactions on Magnetics*, vol. 42, no. 4, pp. 1291–1294, Apr. 2006. DOI: 10.1109/tmag.2006.872412.

[15] W. Sarjeant, "Capacitor fundamentals," in *Proceedings of the 19th Electrical Electronics Insulation Conference*, Chicago, IL, USA, Sep. 1989. DOI: 10.1109/eeic.1989.208190.

[16] M. Stojanovic, "Study and modeling of inter-component coupling for filter design: Application to automotive EMI filters," Ph.D. dissertation, Electronique, INSA de Rennes, 2018.

[17] N. S. Murthy, *SEMI receiver*, Valeo Siemens eAutomotive Germany GmbH, Erlangen, Germany, 2021.

[18] CISPR16-1-1. "Specification for radio disturbance and immunity measuring apparatus and methods - part 1-1: Radio disturbance and immunity measuring apparatus - measuring apparatus," International Electrotechnical Commission.